Journal of Applied Engineering and Technological Science
Vol 5(2) 2024: 1232-1241

PREPARATION, SYNTHESIS AND CHARACTERIZATION OF $La_{(1x)}Sr_{(x)}MnO_3$ ALLOY

Ramlan[1], Fatma Husaini[2], Jan Setiawan[3*], Ferry Budhi Susetyo[4], Hamdan Akbar Notonegoro[5], Silviana Simbolon[6], Dwi Nanto[7], Yunasfi[8]
Department of Physics, Universitas Sriwijaya, Sumatera Selatan, Indonesia[12]
Department of Electrical Engineering, Universitas Pamulang, Tangerang Selatan, Indonesia[3]
Department of Mechanical Engineering, Universitas Negeri Jakarta, Jakarta, Indonesia[4]
Department of Mechanical Engineering, Universitas Sultan Ageng Tirtayasa, Cilegon, Indonesia[5]
Department of Mechanical Engineering, Universitas Pamulang, Tangerang Selatan, Indonesia[6]
Department of Physic Education, Universitas Islam Negeri Syarif Hidayatullah, Jakarta, Indonesia[67]
Research Center for Advanced Material-National Research Innovation Agency, Tangerang Selatan, Indonesia[38]
dosen01647@unpam.ac.id

Received : 23 December 2023, Revised: 18 March 2024, Accepted : 23 March 2024
**Corresponding Author*

ABSTRACT
Magnetic particles have been used for hyperthermia by inserting ferromagnetic material into tumor tissue. $La_{(1-x)}Sr_{(x)}MnO_3$ is one of the best candidates for hyperthermia due to higher magnetic at ambient temperature and their Curie temperature easily adjusted. This research synthesized $La_{(1-x)}Sr_{(x)}MnO_3$ using the ball milling technique. Several heat treatments were also conducted after ball milling processing. Various investigations, including SEM-EDS, XRD, DSC, and VSM, were conducted. $LaMnO_3$ has a hexagonal structure, which has the space group R -3 c. From the diffraction pattern seen in $LaMnO_3$ and $La_{0.9}Sr_{0.1}MnO_3$ seen at angles 32.376 and 32.706, it looks separate like the database diffraction pattern. In $La_{0.9}Sr_{0.1}MnO_3$, these two peaks are seen to be increasingly separated. In contrast to the diffraction patterns of $La_{0.7}Sr_{0.3}MnO_3$ and $La_{0.5}Sr_{0.5}MnO_3$ at an angle of 32.376, there is a decrease in intensity. The specific heat capacity of the alloy with Sr substitution of 0.3 has a greater value than that without substitution and the lowest occurs in the alloy with Sr substitution of 0.1. The magnetization value for Sr substitution is 0.3 higher than for other alloys.
Keywords : *Powder, Crystallographic orientation, Magnetic, Heat capacitance, Morphology*

1. Introduction

Human cancer disease is one of the most fatal in the world after cardiovascular disease (Jadhav et al., 2017). Three standard methods to treat cancer include chemotherapy, radiotherapy, and chemotherapy, but none are satisfied (Yagawa et al., 2017). Over the past decade, the survival rate of cancer survivor patients has increased (Miller et al., 2019, 2022). This condition cannot be separated from the development of hyperthermia. The heat treatment approach in cancer therapy is known as hyperthermia (Yi et al., 2022). Hyperthermia could cause minimal damage to healthy tissue (Jadhav et al., 2017). For cancer treatment, hyperthermia is commonly used in combination with chemotherapy, immunotherapy, and radiotherapy, but it is possible to use hyperthermia alone (Cheng et al., 2019).

Magnetic particles have been used for hyperthermia by inserting ferromagnetic material into tumor tissue and then applying an alternating magnetic field (AMF). By applying an AMF, the temperature of the ferromagnetic material could rise (Manh et al., 2014). Cancer cells could be irreversibly destroyed at between 43 – 45 °C, while normal cells at 46 °C can survive (Konopacki et al., 2021; Manh et al., 2014). However, a significant challenge to scientists is heating cancer cells without damaging the normal cells. Several investigations for the fabrication process and composition in the material could respond to this challenge. $La_{(1-x)}Sr_{(x)}MnO_3$ is one of the best candidates for hyperthermia due to better properties. Some researcher used sol-gel, solution combustion, or milling to fabricated the alloy. The milling process is a promising candidate for low-cost synthesis and the ability to achieve lower grain

size at room temperature. Beside fabrication process, Sr content in the alloy also could enhanced properties such as Curie temperature (Epherre et al., 2011).

Based on those mentioned above, milling, heat treatment methods, and Sr content are needed for deep exploration in $La_{(1-x)}Sr_{(x)}MnO_3$ synthesis, especially for comprehensive material characterization such as surface morphology, phase forming, thermal behavior, and magnetic behavior. This research synthesized $La_{(1-x)}Sr_{(x)}MnO_3$ using the ball milling technique and various heat treatments. In addition, several Sr and La compositions also vary in the alloy due to different research focused on $La_{0.7}Sr_{0.3}MnO_3$.

2. Literature Review

Recently, a wide range of ferromagnetic materials have been used in applications for hyperthermia (Jadhav et al., 2017; Konopacki et al., 2021; Talaat et al., 2016; B. Wang et al., 2018). $La_{(1-x)}Sr_{(x)}MnO_3$ is one of the best candidates for hyperthermia due to higher magnetic at ambient temperature and their Curie temperature easily adjusted (Apostolov et al., 2018; Jadhav et al., 2017). $La_{(1-x)}Sr_{(x)}MnO_3$ could be synthesized using sol-gel, solution combustion, or milling. Generally, the fabrication method could influence the structure, phase composition, grain, and lattice parameters that affect the material's properties (Duan et al., 2016).

Duan et al. synthesized $La_{0.67}Sr_{0.33}MnO_3$ using sol-gel, resulting in Ms 586 emu/cm^3 (Duan et al., 2016). Flores Urquizo et al. synthesize $La_{0.7}Sr_{0.3}MnO_3$ using urea and glycin solution combustion, resulting in 36 to 63 nm and 20 to 45 nm particle size (Flores Urquizo et al., 2020). Campillo et al. synthesized $La_{1-x}Sr_xMnO_3$ (x=0.3 and x=0.4) using ball milling, resulting in a shift to more duration milling time, less crystallite size was formed. Moreover, less La and higher Sr promote a lower crystallite size (Campillo et al., 2019). Manh et al. synthesized $La_{0.7}Sr_{0.3}MnO_3$ using reactive milling combined with a thermal processing method, resulting in various crystallite sizes (20, 30, and 40 nm). Shifting to a more crystallite size increases Ms (Manh et al., 2014). Manh et al. synthesized $La_{0.7}Sr_{0.3}MnO_3$ using a similar method in a 2014 study with various calcined at 4 h (700 and 800 ◦C). They found that shifting to a higher temperature increased crystallite and particle size (Manh et al., 2023). Figueroa et al. synthesize $La_{0.7}Sr_{0.3}MnO_3$ using the ball milling method at various milling time durations, resulting in less crystallite size with increased milling duration time and coercivity field increase with milling time at 5K (Figueroa et al., 2014).

Sr content in the alloy also contributed to the properties of the material. Bork et al. found that increasing the Sr could enhance oxygen release and hydrogen production (Bork et al., 2017). Das et al. have found that an increase in Sr content leads to an increase in density and a decrease in crystallite size (Das et al., 2017). Wang et al. have found that increased Sr content leads to increase surface area and reduced pore diameters (M. Wang et al., 2021).

3. Experimental Methods

La_2O_3, $SrCO_3$, and MnO_2 powder are obtained from Merck (purity ≥99%) as a precursor for La, Sr, and MnO. $La_{(1-x)}Sr_{(x)}MnO_3$ alloy was prepared using a milling process with x are 0.1, 0.3, and 0.5. The milling process was conducted at speed 1500 rpm for 5 h, placing powder in acetone at room temperature. Afterward, the powder was dried in the vial, heated in the oven for 12 h at 80 ◦C in air. Dried powder was compacted at 20 tons and sintered in the furnace for 12 h at 1200 ◦C in air. Then, the sample was crushed in the agate mortar, for powder homogeneity stainless steel screen with 400 mesh was used. The achieved powder used for further investigation. The complete experimental procedure can be seen in Figure 1.

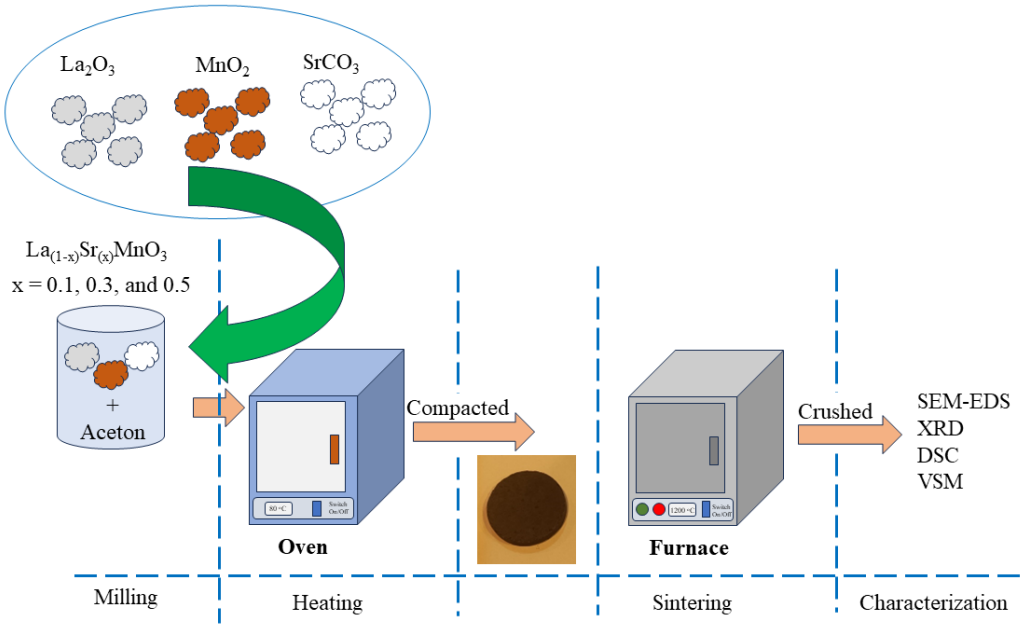

Fig. 1. Schematic representation of experimental method.

The Surface morphology and element analysis of the samples using Scanning Electron Micoscope (SEM) JEOL JSM 6510. The SEM images showed how the substitution element changes the morphology. The Energy Dispersive X-ray Spectroscopy (EDS) would confirm the elemental compositions on the surface of material. the X-ray Diffraction (XRD) was obtained using PANalytical AERIS with CuKα radiation (λ=1.5406 Å). XRD data was collected using step size 0.02° for diffraction angle from 20 – 80° at room temperature. XRD patterns were analyzed by Rietveld refined analysis using Highscore Plus software equipped database International Centre for Diffraction Data (ICDD), Inorganic Crystal Structure Database (ICSD), and Crystallography Open Database (COD). These diffraction data obtained to showing the formation of single phase or more. The material with single phase are more desireable. Heat capacitances of lanthanum manganites were checked using DSC Perkin Elmer DSC 4000 from -15 to 75 °C with a heating rate of 5°C/min. heat capacities would show how much energy that needed for the sample increases their temperatiure for 1°. While magnetic properties of the samples were investigated using VSM250 up to a field of 20 kOe at room temperature. Through the magnetic properties,would show the behaviour of the saturation, remanent and coercive filed of magnetic in the samples.

4. Results and Discussions

4.1 SEM-EDS

SEM and EDS were conducted to analyze the morphology and elemental of the samples. SEM equipped with EDS results of various samples is presented in Figure 2.

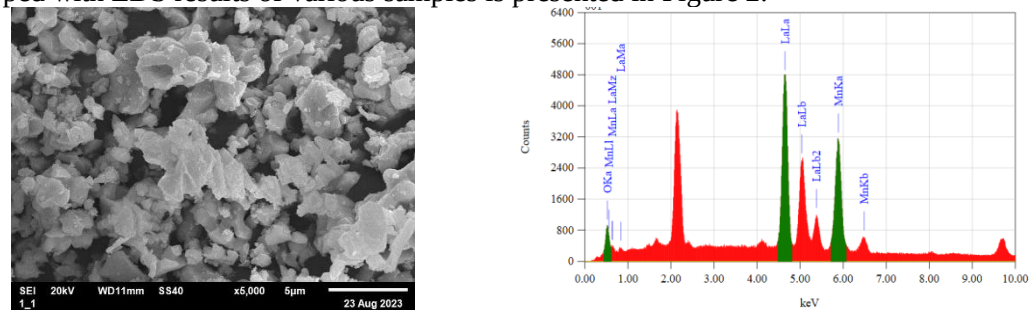

(a)

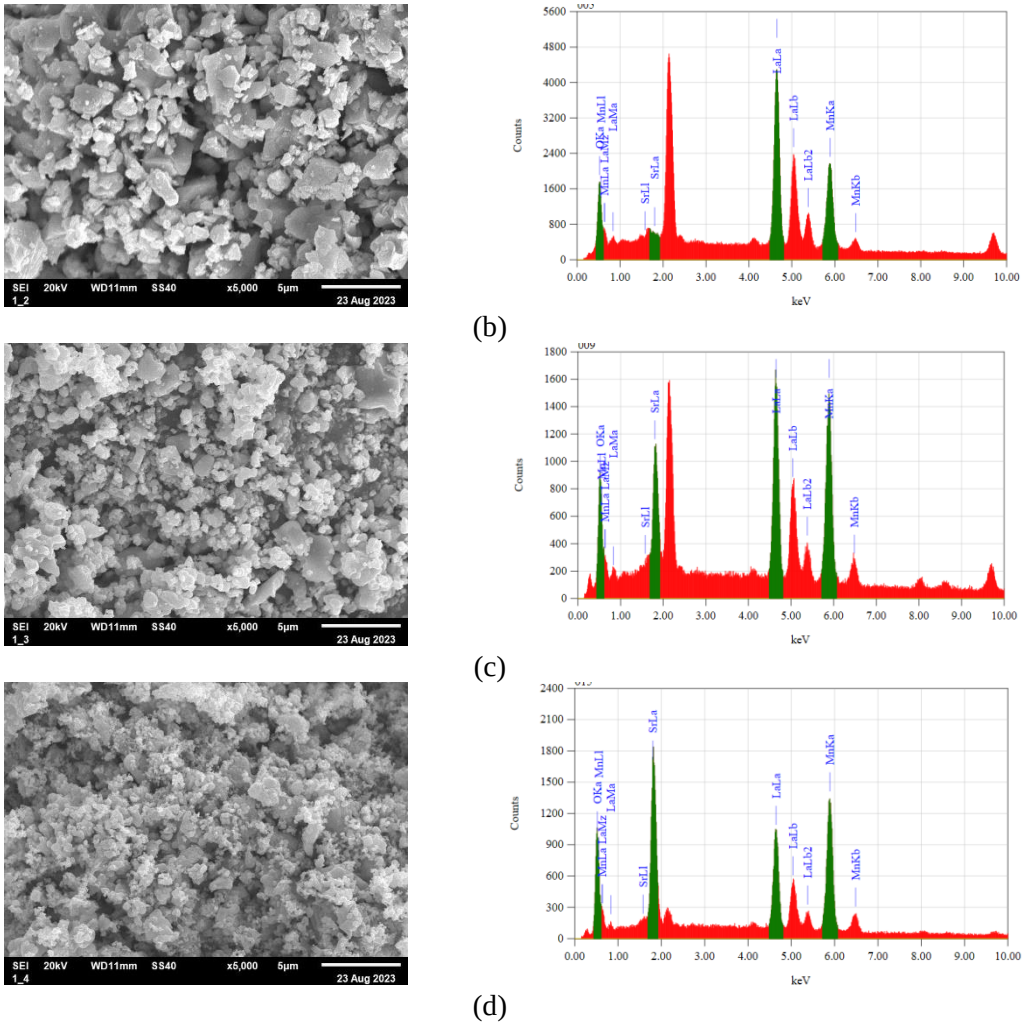

Fig. 2. Morphology and EDS spectrum characterization result of $La_{(1-x)}Sr_{(x)}MnO_3$ powder with x (a) 0, (b) 0.1, (c) 0.3, and (d) 0.5.

Based on Figure 2, the alloy powder gets finer by increasing the composition of Sr. Ouhaibi et al. research found similar results to the present research, increasing the Sr promoted to get fine morphology (Ouhaibi et al., 2018). The tendency to better agglomerate is also visible in Figure 2, which perfectly agrees with Das et al.'s result (Das et al., 2017). Better agglomeration and finer grain give a tendency to more compact morphology.

Table 1 - EDS element at (wt.%) analysis result of the $La_{(1-x)}Sr_{(x)}MnO_3$.

Element	x			
	0	0.1	0.3	0.5
La	70.53	70.98	50.25	36.53
Sr	-	1.76	13.40	22.41
Mn	26.29	20.17	27.35	27.58
O	3.19	7.09	8.99	13.48

From the EDS spectrum (Figure 2), it can be seen that the elements La and Mn dominate, and there are some Sr elements. The Sr element can be observed in the range 1 – 2 keV with the SrLa and SrL1 spectra. With Sr substitution with an amount of 0.1, the spectrum of the Sr element is not very visible, probably because the area analyzed does not contain the correct Sr elements. Meanwhile, the element spectrum is more visible for larger amounts of Sr substitution (0.3 and 0.5). The complete EDS measurement result is seen in Table 1. Based on Table 1, it can be seen Sr is a perfect substitute for the $LaMnO_3$ alloy.

4.2 XRD

XRD patterns were analyzed using Rietveld's refined analysis. Highscore Plus software is used for Rietveld refine analysis. A complete XRD curve or various samples can be seen in Figure 3. According to Figure 3, it can be seen that each peak in the sample corresponds to the

peak in the ICSD database card 98-005-5965 for $LaMnO_3$ with a hexagonal structure which has the space group R -3 c, which perfectly agrees with Manh et al. report (Manh et al., 2014). The diffraction pattern in $LaMnO_3$ and $La_{0.9}Sr_{0.1}MnO_3$ at angles 32.376 and 32.706 looks separate, like the database diffraction pattern. In $La_{0.9}Sr_{0.1}MnO_3$, these two peaks are seen to be increasingly separated. In contrast to the diffraction patterns of $La_{0.7}Sr_{0.3}MnO_3$ and $La_{0.5}Sr_{0.5}MnO_3$ at an angle of 32.376, there is a decrease in intensity. It can also be seen significantly that the intensity has decreased in several corners, and there is also a widening. Furthermore, Rietveld analysis was carried out using the Highscore Plus software for crystallographic orientation analysis of the diffraction pattern. Table 2 summarizes the results of the Rietveld analysis for the crystal system, space group, lattice parameter, occupancy, and statistical parameters.

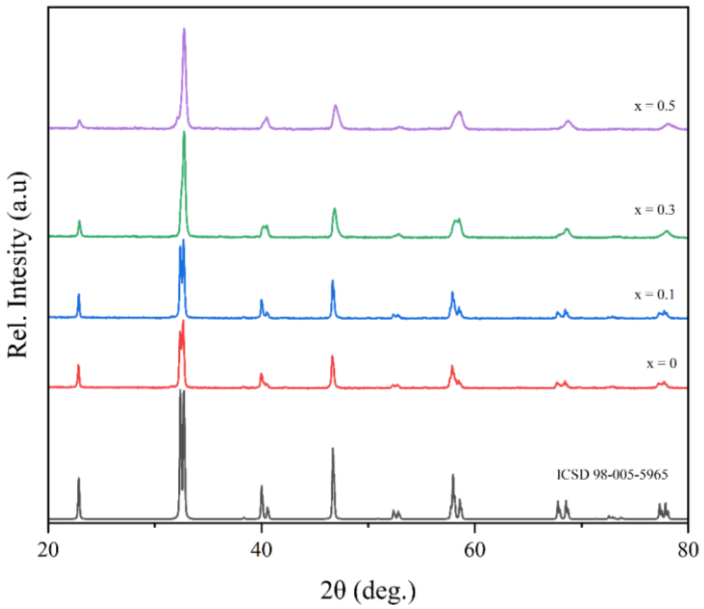

Fig. 3. Diffraction pattern of $La_{(1-x)}Sr_{(x)}MnO_3$ powder.

Table 2 - Rietveld analysis of the $La_{(1-x)}Sr_{(x)}MnO_3$.

Parameter	x			
	0	0.1	0.3	0.5
Crystal system	Hexagonal			
Space group	R -3 c			
Lattice parameter				
a = b [Å]	5.525230	5.526490	5.499280	5.465754
c [Å]	13.36977	13.35858	13.35068	13.36132
Volume [$Å^3$]	353.4720	353.3374	349.6600	345.6820
Crystallite size [nm]	45.5	54.4	28.5	24.3
Density (g/cm^3)	6.82	6.72	6.46	6.24
Occupancy				
La	1	0.927506	0.705424	0.521154
Sr	0	0.072494	0.294576	0.478846
Statistic parameter				
Goodness of fit	2.64816	2.17614	5.28940	2.85393
Rp	3.01445	2.73462	3.24420	2.31739
Rwp	4.09809	3.52004	4.87471	3.27809

Table 2 shows that increased Sr substitution promoted decreased volume and crystallite size. Das et al. found that an increase in the Sr content leads to a decrease in crystallite size (Das et al., 2017). Aina et al. also found behavior similar to the present research (Aina et al., 2013). Ridha et al. found that increased Sr content promoted decreased volume (Ridha et al., 2009). Moreover, compared to the SEM result, increased Sr substitution promoted better agglomeration, and finer grain would correlate to a change in crystallite size. Ouhaibi et al. have found more fine morphology with less crystallite size (Ouhaibi et al., 2018). Therefore, there is a correlation between Sr content and fine morphology, which promotes decreased volume and crystallite size.

4.3 DSC

DSC was investigated at temperatures -15 to 75 °C. The results of the DSC investigation can be seen in Figure 4.

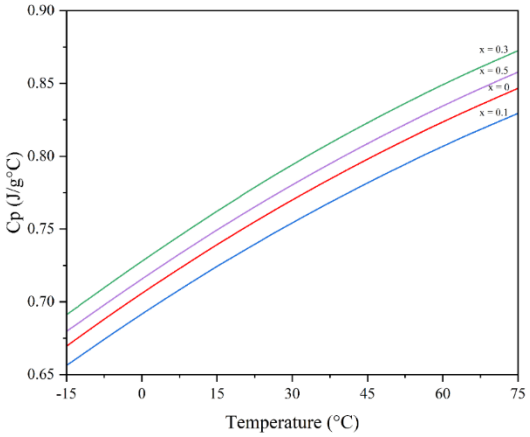

Fig. 4. Heat capacitance (Cp) of $La_{(1-x)}Sr_{(x)}MnO_3$.

According to Figure 4, the alloy's specific heat capacity depends on the temperature. With an increase in temperature, heat capacity also increases. The specific heat capacity of the alloy with Sr substitution of 0.3 has a greater value than that without substitution, and the lowest occurs in the alloy with a Sr substitution of 0.1. This specific heat capacity parameter shows how much energy per mass is needed to increase the temperature of the material by 1 °C. The higher the specific heat capacity value, the greater the energy required per mass to increase the temperature. Meanwhile, a low specific heat capacity value only requires a small amount of energy per mass to increase the temperature. Based on the heat capacity values in Figure 4 for the range -15 to 75, the $La_{0.7}Sr_{0.3}MnO_3$ alloy has the highest value. According to Khlopkin et al., at temperature 300 K (±27 °C), $La_{0.8}Sr_{0.2}MnO_3$ has the highest value, followed by $La_{0.7}Sr_{0.3}MnO_3$ and $LaMnO_3$. But in temperatures around 120 K (±153°C), $LaMnO_3$ has more heat capacitance than others (Khlopkin et al., 2000). Moreover, according to Bork et al., which investigated $La_{1-x}Sr_xMnO_3$ (x=0.2, 0.3 and 0.4) at 1200-1800K (±927- ±1526°C), found that increasing Sr content led to increasing heat capacity (Bork et al., 2017). Therefore, specific heat capacity depends on temperature and Sr composition.

4.4 VSM

Magnetic properties of the samples were investigated using VSM250 up to a field of 20 kOe at room temperature. VSM results are presented in Figures 4 and 5. Their characteristic of magnetic hysteresis curved in Fig. 5 showed the S-shaped. The narrow of S-shaped curve confirm that Sr changes the lanthanum manganite become the soft magnetic behaviour in nature.

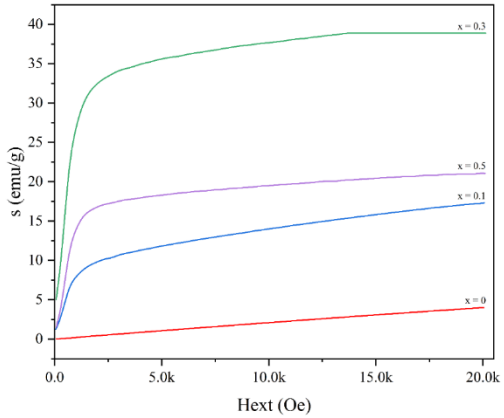

Fig. 5. Magnetization of $La_{(1-x)}Sr_{(x)}MnO_3$ powder.

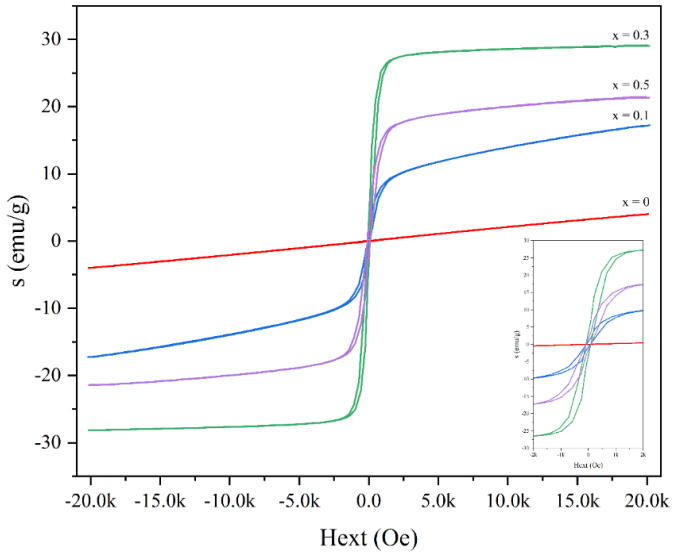

Fig. 6. Hysteresis curve of $La_{(1-x)}Sr_{(x)}MnO_3$ powder.

The magnetic characteristic test results in Figure 4 and Figure 5 (Summarize in Table 3) show that the magnetization value (Ms) for Sr substitution is 0.3 higher than for other alloys. From Figure 5, Ms in the alloy with Sr substitution of 0.3 is 29.15 emu/g. The mechanism for changing the magnetic value of the $La_{(1-x)}Sr_{(x)}MnO_3$ alloy is greatly influenced by the amount of Sr substitution, which will provide the optimum magnetization value. There are compositions with specific values that can provide maximum magnetic characteristics, but other compositions that may be higher will reduce the magnetic characteristics.

Wang et al. added various Sr (x= 0, 0.05, 0.1, and 0.15) in the $Y_{1-x}Sr_xFeO_3$ and found increasing Sr content led to an increase in Mr and Ms (M. Wang et al., 2021). Bai et al. have added Sr content (x=0.5, 1, 1.5 and 2) to $Ba_{2-x}Sr_xZn_{1.2}Co_{0.4}Cu_{0.4}Fe_{12}O_{22}$, found Ms for x= 0.5 to 1.5 relatives similar value, similar behavior also found for Mr value. At x= 2, Mr and Ms increased sharply (Bai et al., 2005). Moreover, another study found that optimum conditions for Mr and Ms are 70.1 and 42.4 emu/g at 11.5 Fe/Sr addition (Y. Wang et al., 2009). Based on several findings, it was corroborated that Sr addition has an optimum condition to reach a maximum magnetization value.

Table 3 - VSM result of the $La_{(1-x)}Sr_{(x)}MnO_3$.

x	Mr (emu/g)	Ms (emu/g)	Hc (Oe)
0	0.02	4.02	105.18
0.1	0.86	17.26	75.73
0.3	3.32	29.15	86.17
0.5	1.75	21.48	93.33

The addition of Sr at 0.1, 0.3, and 0.5 results in a finer morphology with smaller grains. The elemental composition also shows the distribution of Sr, which follows a trend based on the amount of substitution. XRD confirms that only one phase is formed, the LaMnO3 phase, implying that Sr substitutes La. The Rietveld analysis shows that the crystallite size with Sr of 0.1 is larger than without Sr substitution. This phenomenon is followed by a lower heat capacity for Sr of 0.1 when compared to other quantities. However, remanence and magnetic saturation show that Sr 0.3 has superior properties to the others. The magnetic properties of Sr 0.3 provide an advantage, but the magnetic heating process may require a significant amount of energy. When viewed differently, this sample will exhibit more consistent temperature stability across a broader range of applicable magnetic field compared to other Sr substitutions.

5. Conclusion

The $La_{(1-x)}Sr_{(x)}MnO_3$ alloy could be well synthesized. X-ray diffraction, morphology, and elemental content analysis results corroborate this statement. Increasing the Sr content would influence the reach to fine morphology, which promotes decreased volume and crystallite size. The specific heat capacity depends on temperature and Sr composition. Regarding its function as a magnetic material, the alloy with Sr = 0.3 doped shows superior characteristics compared to

alloys without doping and other synthesized substitutes. This alloy also shows superiority over other alloys in terms of heat capacity characteristics.

Acknowledgement

The author would like to thank Universitas Pamulang, the Ministry of Education, Culture, Research and Technology and National Research Innovation Agency for their support. This activity was funded through research grant funding from the Ministry of Education, Culture, Research and Technology in 2023 with contract number 180/E5/PG.02.00.PL/2023; 021/SP2H/RT-MONO/LL4/2023; 107/D5/SK/LPPM/UNPAM/VII/2023.

References

Aina, V., Bergandi, L., Lusvardi, G., Malavasi, G., Imrie, F. E., Gibson, I. R., Cerrato, G., & Ghigo, D. (2013). Sr-containing hydroxyapatite: Morphologies of HA crystals and bioactivity on osteoblast cells. *Materials Science and Engineering C*, *33*(3), 1132–1142. https://doi.org/10.1016/j.msec.2012.12.005

Apostolov, A. T., Apostolova, I. N., & Wesselinowa, J. M. (2018). La1−xSrxMnO3 Nanoparticles for Magnetic Hyperthermia. *Physica Status Solidi (B) Basic Research*, *255*(6), 1–15. https://doi.org/10.1002/pssb.201700587

Bai, Y., Zhou, J., Gui, Z., & Li, L. (2005). The effect of Sr substitution on phase formation and magnetic properties of Y-type hexagonal ferrite. *Journal of the American Ceramic Society*, *88*(2), 318–323. https://doi.org/10.1111/j.1551-2916.2005.00080.x

Bork, A. H., Povoden-Karadeniz, E., & Rupp, J. L. M. (2017). Modeling Thermochemical Solar-to-Fuel Conversion: CALPHAD for Thermodynamic Assessment Studies of Perovskites, Exemplified for (La,Sr)MnO3. *Advanced Energy Materials*, *7*(1). https://doi.org/10.1002/aenm.201601086

Campillo, G., Osorio, J., Arnache, O., Gil, A., Beltrán, J. J., & Dorkis, L. (2019). Grain Size Reduction Effect on Structural and Magnetic Properties in La1-xSrxMnO3 (x = 0.3 y 0.4) by Mechanical Ball Milling. *Journal of Physics: Conference Series*, *1247*(1), 0–6. https://doi.org/10.1088/1742-6596/1247/1/012015

Cheng, Y., Weng, S., Yu, L., Zhu, N., Yang, M., & Yuan, Y. (2019). The Role of Hyperthermia in the Multidisciplinary Treatment of Malignant Tumors. *Integrative Cancer Therapies*, *18*. https://doi.org/10.1177/1534735419876345

Das, T., Das, B. K., Parashar, K., Kumar, R., Choudhary, H. K., Anupama, A. V., Sahoo, B., Sahoo, P. K., & Parashar, S. K. S. (2017). Effect of Sr-doping on sinterability, morphology, structure, photocatalytic activity and AC conductivity of ZnO ceramics. *Journal of Materials Science: Materials in Electronics*, *28*(18), 13587–13595. https://doi.org/10.1007/s10854-017-7198-6

Duan, Z., Cui, Y., Shi, X., Wei, J., Ren, P., & Zhao, G. (2016). Facile fabrication of micro-patterned LSMO films with unchanged magnetic properties by photosensitive sol-gel method on LaAlO3 substrates. *Ceramics International*, *42*(12), 14100–14106. https://doi.org/10.1016/j.ceramint.2016.06.021

Epherre, R., Pepin, C., Penin, N., Duguet, E., Mornet, S., Pollert, E., & Goglio, G. (2011). Evidence of non-stoichiometry effects in nanometric manganite perovskites: Influence on the magnetic ordering temperature. *Journal of Materials Chemistry*, *21*(38), 14990–14998. https://doi.org/10.1039/c1jm12137e

Figueroa, G. C., Olmos, Ó. A., Garcés, A. G., Vélez, J. A. O., Beltrán, J. J., Miranda, E. B., & Castillo, R. (2014). Influence of Ball Milling Process on Structural and Magnetic Properties of OF La0.7Sr0.3MnO3 Manganite. *Revista EIA*, *11*, 31–38.

Flores Urquizo, I. A., Sanchez Correa, H., Montes De Oca Ayala, F. T., Rivera De La Rosa, J., & Hernandez Garcia, T. C. (2020). Synthesis of La-Sr-Mn-O and La-Sr-Ca-Mn-O Perovskites through Solution Combustion Using Urea at Fuel Deficient Conditions. *IEEE Transactions on Nanobioscience*, *19*(2), 183–191. https://doi.org/10.1109/TNB.2019.2963703

Jadhav, S. V., Lee, S. H., Nikam, D. S., Bohara, R. A., Pawar, S. H., & Yu, Y. S. (2017). Studies on enhanced colloidal stability and heating ability of glycine functionalized

LSMO nanoparticles for cancer hyperthermia therapy. *New Journal of Chemistry*, *41*(4), 1598–1608. https://doi.org/10.1039/c6nj03384a

Khlopkin, M. N., Panova, G. K., Shikov, A. A., Sinyavskiĭ, V. F., & Shulyatev, D. A. (2000). Heat capacity of La1-xSrxMnO3 single crystals in different magnetic states. *Physics of the Solid State*, *42*(1), 114–119. https://doi.org/10.1134/1.1131177

Konopacki, M., Jędrzejczak-Silicka, M., Szymańska, K., Mijowska, E., & Rakoczy, R. (2021). Effect of rotating magnetic field on ferromagnetic structures used in hyperthermia. *Journal of Magnetism and Magnetic Materials*, *518*(September 2020), 167418. https://doi.org/10.1016/j.jmmm.2020.167418

Manh, D. H., Ngoc Nha, T. T., Hong Phong, L. T., Nam, P. H., Thanh, T. D., & Phong, P. T. (2023). Determination of the crystalline size of hexagonal La1−xSrxMnO3 (x = 0.3) nanoparticles from X-ray diffraction - a comparative study. *RSC Advances*, *13*(36), 25007–25017. https://doi.org/10.1039/d3ra04018f

Manh, D. H., Phong, P. T., Nam, P. H., Tung, D. K., Phuc, N. X., & Lee, I. J. (2014). Structural and magnetic study of La0.7Sr0.3MnO 3 nanoparticles and AC magnetic heating characteristics for hyperthermia applications. *Physica B: Condensed Matter*, *444*, 94–102. https://doi.org/10.1016/j.physb.2014.03.025

Miller, K. D., Nogueira, L., Devasia, T., Mariotto, A. B., Yabroff, K. R., Jemal, A., Kramer, J., & Siegel, R. L. (2022). Cancer treatment and survivorship statistics, 2022. *CA: A Cancer Journal for Clinicians*, *72*(5), 409–436. https://doi.org/10.3322/caac.21731

Miller, K. D., Nogueira, L., Mariotto, A. B., Rowland, J. H., Yabroff, K. R., Alfano, C. M., Jemal, A., Kramer, J. L., & Siegel, R. L. (2019). Cancer treatment and survivorship statistics, 2019. *CA: A Cancer Journal for Clinicians*, *69*(5), 363–385. https://doi.org/10.3322/caac.21565

Ouhaibi, A., Ghamnia, M., Dahamni, M. A., Heresanu, V., Fauquet, C., & Tonneau, D. (2018). The effect of strontium doping on structural and morphological properties of ZnO nanofilms synthesized by ultrasonic spray pyrolysis method. *Journal of Science: Advanced Materials and Devices*, *3*(1), 29–36. https://doi.org/10.1016/j.jsamd.2018.01.004

Ridha, N. J., Yunus, W. M. M., Halim, S. A., Talib, Z. A., Al-Asfoor, F. K. M., & Primus, W. C. (2009). Effect of Sr Substitution on Structure and Thermal Diffusivity ofBa1-xSrxTiO3 Ceramic. *American Journal of Engineering and Applied Sciences*, *2*(4), 661–664. https://doi.org/10.3844/ajeassp.2009.661.664

Talaat, A., Alonso, J., Zhukova, V., Garaio, E., García, J. A., Srikanth, H., Phan, M. H., & Zhukov, A. (2016). Ferromagnetic glass-coated microwires with good heating properties for magnetic hyperthermia. *Scientific Reports*, *6*(December), 1–6. https://doi.org/10.1038/srep39300

Wang, B., Chan, K. F., Yu, J., Wang, Q., Yang, L., Chiu, P. W. Y., & Zhang, L. (2018). Reconfigurable Swarms of Ferromagnetic Colloids for Enhanced Local Hyperthermia. *Advanced Functional Materials*, *28*(25), 1–12. https://doi.org/10.1002/adfm.201705701

Wang, M., Cheng, L., Huang, L., Pan, S., Yao, Q., Hu, C., Liang, Q., & Zhou, H. (2021). Effect of Sr doped the YFeO3 rare earth ortho-ferrite on structure, magnetic properties, and microwave absorption performance. *Ceramics International*, *47*(24), 34159–34169. https://doi.org/10.1016/j.ceramint.2021.08.325

Wang, Y., Li, Q., Zhang, C., & Li, B. (2009). Effect of Fe/Sr mole ratios on the formation and magnetic properties of SrFe12O19 microtubules prepared by sol-gel method. *Journal of Magnetism and Magnetic Materials*, *321*(19), 3368–3372. https://doi.org/10.1016/j.jmmm.2009.05.066

Yagawa, Y., Tanigawa, K., Kobayashi, Y., & Yamamoto, M. (2017). Cancer immunity and therapy using hyperthermia with immunotherapy, radiotherapy, chemotherapy, and surgery. *Journal of Cancer Metastasis and Treatment*, *3*(10), 218. https://doi.org/10.20517/2394-4722.2017.35

Yi, G. Y., Kim, M. J., Kim, H. I., Park, J., & Baek, S. H. (2022). Hyperthermia Treatment as a Promising Anti-Cancer Strategy: Therapeutic Targets, Perspective Mechanisms and Synergistic Combinations in Experimental Approaches. *Antioxidants*, *11*(4).

https://doi.org/10.3390/antiox11040625